Steady-State Thickness of Liquid–Gas Foams

Laurent Pilon,* Andrei G. Fedorov,† and Raymond Viskanta*,1

*Heat Transfer Laboratory, School of Mechanical Engineering, Purdue University, West Lafayette, Indiana 47907; and †Multiscale Integrated
Thermofluidics Laboratory, G. W. Woodruff School of Mechanical Engineering, Georgia Institute of Technology, Atlanta, Georgia 30332-0405

**This paper presents an approach for predicting the thickness
of isothermal foams produced by blowing gas in a liquid solution under steady-state conditions. The governing equation for
the transient foam thickness has been nondimensionalized, and
two-dimensionless numbers have been identified to describe the
formation and stability of this type of foam: $\Pi_1 = Re/Fr$ and
$\Pi_2 = CaH_\infty/r_0$. Physical interpretation of the dimensionless numbers has been proposed; a power-law type relation has been assumed
between Π_1 and Π_2 (i.e., $\Pi_2 = K\Pi_1^n$). Experimental data available in the literature have been used to determine the empirical
parameters of the correlation K and n. The experimental conditions cover a wide range of viscosity, density, surface tension, gas
superficial velocity, and average bubble radius. The model is valid
for foams formed from high-viscosity liquids bubbled with nitrogen,
air, helium, hydrogen, and argon injected through single, multiorifice nozzles or porous medium. A comparison between the correlation developed and the experimental data yields reasonable agreement (within 35% error), given the broadness of the bubble radius
distribution around the mean value and the uncertainty of the experimental data and of the thermophysical properties. Predictions
have been found to be very sensitive to the average bubble radius.
A more refined model is still needed which should be supported
by careful experimental studies. Finally, suggestions are given to
extend the present work to foams generated from low-viscosity
solutions.**   © 2001 Academic Press

Key Words: **foam thickness; steady foam; pneumatic foam; semibatch foam; glass foam; slag foaming; bath smelting.**

INTRODUCTION

Pneumatic foams are produced by a continuous stream of gas
bubbles rising to the surface of a foaming liquid. Such foams
are encountered in a number of practical technological systems
ranging from glass-, iron-, and steel-making processes to protein separation and bioreactors. Bubbles are either generated
by chemical reactions taking place within the liquid or injected
in the liquid through a single nozzle, a multinozzle inlet, or a
porous medium (e.g., frit ceramic (17)). In experimental studies,
chemical reactions are often simulated by injecting gas in the solution to permit better control and measure of the gas flow rate

(34); however, such a simulation is only partial since bubbles
generated by chemical reactions tend to be smaller than bubbles
generated by gas injection (34).

In bioreactors, bubbles are generated by an air sparger placed
beneath the agitator to aerate the culture medium (3). In the
presence of surface-active agents, foam may be formed and act
as a cushion, preventing bursting bubbles from damaging the
cells at the liquid surface. In electric arc furnaces, foam is often
required to shield the refractories from the arc, to protect the
liquid metal from the atmosphere (29), and to help stabilize the
arc in modern electric arc furnaces (29). Controlling foam is also
important in other steel-making processes such as basic oxygen
smelting (BOS) and the making of iron by bath smelting (31).
In glass-melting furnaces, foam produced by chemical reactions
taking place within the melt is often undesirable since it reduces
significantly heat transfer rates from the combustion space to the
melt (7, 20, 21), thereby increasing the operating temperature,
the NO_x-formation rate, and the energy consumption (21).

Understanding and modeling of the foam thickness is, therefore, of major importance from both fundamental and practical
viewpoints. This paper is concerned with the analysis of steady-state foams, i.e., when the burst of the bubbles at the top of the
foam is compensated by the supply of bubbles at the bottom. The
objective is to develop a model for predicting the steady-state
foam thickness as a function of the thermophysical properties of
the system, the bubble size, and the superficial gas velocity. The
effects of the temperature (uniform across the foam), the initial
liquid height, and the type of gas are investigated as well.

ANALYSIS

Current State of Knowledge

The first model predicting the steady-state foam height as a
function of the superficial gas velocity j[2] has been proposed
by Bikerman (2). He suggested that below a critical superficial
gas velocity j_{cr}, the steady-state foam thickness H_∞ increases
linearly with the gas flux,

$$H_\infty = \Omega j \quad \text{if } j \le j_{cr}, \qquad [1]$$

---

[2] The superficial gas velocity is defined as the gas flow rate in m^3/s divided
by the cross-sectional area of the container in m^2.

where Ω is a constant called the "unit of foaminess" or "foaming index" and is considered to be a physical characteristic of the liquid corresponding to the residence time of a bubble in the foam. Beyond the critical mass flux j_{cr}, the entrainment of the liquid into the foam by rising bubbles cannot be balanced by drainage and the foam thickness increases without limit. However, experimental data for viscous oils (14, 23) indicate that the transition from a steady-state foam to a constantly growing foam is not abrupt at $j = j_{cr}$ but continuous, thereby indicating that the "unit of foaminess" Ω in Eq. [1] is not constant but increases as the mass flux j increases. Lin and Guthrie (22) observed that, for low gas influx, a bubbly flow prevails, bubbles are small and spherical or ellipsoidal, and the foam thickness increases linearly with the superficial gas velocity; i.e., Eq. [1] is valid. However, for higher gas influx, bubbles coalesce and a churn-turbulent flow regime is observed with spherical-cap bubbles forming while rising to the surface, and the foam tends to be unstable, i.e., the foam thickness decreases with the gas flow rate. Moreover, Laimbock (21) has observed that foaming of soda-lime silicate glass at different temperatures was not possible for an arbitrarily small gas flow rate; instead, a minimum superficial gas velocity, j_m, should be reached to initiate foaming. The same observations have been made for different solutions of water and glycerol (9, 17). Application of Eq. [1] to actual iron smelters was also questioned by Lin and Guthrie (22); therefore, Eq. [1] does not appear to be a general and satisfactory relation for describing the foaming behavior of liquids.

Jeelani *et al.* (17) proposed a model for the steady-state foam thickness accounting for the binary coalescences taking place within the foam. The steady-state foam thickness was expressed as a function of the thermophysical properties of the liquid phase, the binary coalescence time, and the average foam porosity. The binary coalescence time as well as the average foam porosity were determined experimentally from the measurements of the average bubble diameter along the foam height. Good agreement was found between the model's predictions and the experimental data for aqueous foams stabilized with glycerinate and surfactants. Unfortunately, most of the other experimental studies of steady-state foam thickness did not provide the variation of the average bubble diameter along the foam height and neither the binary coalescence time nor the average foam porosity can be determined, making it impossible to validate the model for other solutions.

More recently, Hrma (14) developed a model for a steady-state foam blanket. The foam behavior is described in terms of two limiting gas fluxes: the threshold flux j_m corresponding to the minimum gas flux required to generate foam and the critical flux j_{cr} corresponding to the breakdown of steady-state conditions. Then, three different regimes can be identified: (1) If $j < j_m$, the gas flux j reaching the liquid surface is not sufficient to create a foam layer. If $j = j_m$, the foam layer consists of a monolayer of bubbles whose thickness is $2r_0$, where r_0 is the average radius of the bubbles. (2) If $j_m < j \leq j_{cr}$, the foam is steady and its thickness increases as the gas influx increases according to the

following expression (14),

$$H_\infty = 2r_0 + 2r_0 b_h \left[\frac{1/j_m - 1/j_{cr}}{1/j - 1/j_{cr}} - 1 \right], \qquad [2]$$

where r_0 is the average radius of bubbles in the foam and b_h is a constant depending on the gravitational drainage and on the survival time of a critically thin film separating the foam from the atmosphere. (3) If $j \geq j_{cr}$, the excess of mass flux over j_{cr} cannot be released at the top of the foam and has to be stored within the foam. Thus, the foam volume grows continuously and a steady state is never reached until all available liquid is dispersed in the foam (14). Beyond a certain mass flux, vent holes may start developing within the foam and the foam thickness stops growing and may even start decreasing (17, 32). Hrma (14) suggested that Eq. [1] proposed by Bikerman (2) is only valid for evanescent foams for which the liquid lamellae separating the bubbles in the foam rupture as soon as the critical thickness of the foam is reached and for very small superficial gas velocity (i.e., $j \ll j_{cr}$). In that case, Eqs. [1] and [2] are equivalent as long as $b_h = 1$ and $\Omega \approx 2r_0/j_m$. Even if Hrma's model (14) provides some insight into the mechanism of foam formation and stability by explaining qualitatively reported experimental data, it cannot be used to predict the steady-state foam thickness due to the lack of either analytical or semi-empirical expressions for the critical mass flux and the parameter b_h as a function of thermophysical properties of the system.

A series of studies on slag foams in iron- and steel-making processes has been carried out to predict the steady-state foam thickness (15, 16, 18, 19, 34–36). Little discussion has been, however, reported about the stabilizing mechanisms occuring in foams generated from molten salt at high temperature. It is believed that their large dynamic viscosity is a major factor in the foam formation and stabilization. All the experiments consisted of bubbling argon in a cylindrical tank containing liquid CaO–SiO₂–FeO–MgO–Al₂O₃ slags at high temperatures. First, Ito and Fruehan (15) showed that the steady-state foam thickness for CaO–SiO₂–FeO slags is independent of the inside diameter of the container as long as it is larger than 3 cm. They also performed a dimensional analysis based on the Buckingham-Pi theorem to relate the unit of foaminess Ω, the liquid viscosity μ, the liquid density ρ, and the surface tension σ. Two dimensionless numbers were identified, and the foaming index Ω was found to be proportional to the ratio $(\mu/\sqrt{\sigma\rho})$ (16). Jiang and Fruehan (18) confirmed the previous work, but suggested a different empirical constant of proportionality between Ω and $\mu/\sqrt{\sigma\rho}$. However, although the average bubble radius has been identified as an important parameter for the steady-state foam thickness (22), it was not considered in Ito and Fruehan's (15, 16) or in Jiang and Fruehan's (18) work. This point has been recognized by Zhang and Fruehan (34), and the dimensional analysis using Buckingham-Pi theorem has been performed again by adding the average bubble diameter D_0. Three dimensionless groups were identified, and a power type of law was assumed to relate

them. Experimental data suggested the following semi-empirical expression for the unit of foaminess Ω (34):

$$\Omega = 115 \frac{\mu^{1.2}}{\sigma^{0.2} \rho D_0^{0.9}}. \qquad [3]$$

Equation [3] merits further discussion:

• Comparison between the measured and the experimental foam indices Ω for slag foams was plotted on a logarithmic scale (Fig. 17 in Ref. (34)), and after careful analysis, significant discrepancies (up to a factor of 3 between predicted and experimental units of foaminess) have been noted.

• Most of the studies (15, 16, 18, 19, 34–36) rely on the validity of Eq. [1] which seems to be appropriate for slag foams but has been proven erroneous for other foaming solutions (14, 21, 23, 30) (see previous comments about Eq. [1]).

• The semi-empirical Eq. [3] is based on the experimental data obtained for slag foams of similar solutions containing CaO, FeO, SiO_2, MgO, and Al_2O_3, for which thermophysical properties (in particular, the density and the surface tension) and the average bubble diameter do not vary significantly (see Table 1). Thus, the effects of density and surface tension on the steady-state foam thickness were not fully investigated. Therefore, in general, one should not expect Eq. [3] to be valid for other systems having very different thermophysical properties or average bubble diameters.

• Ghag et al. (9) studied pneumatic foams formed by bubbling nitrogen in different solutions containing water, glycerinate (78 to 95 vol%), and SDBS as the surfactant. The authors showed that "there was a poor correlation" between their experimental data and Eq. [3] proposed by Zhang and Fruehan (34). Experimental results indicate that the foaming index predicted by Eq. [3] should be more sensitive to changes in surface tension and that the exponent associated with the average bubble diameter D_0 was a major cause of the discrepancies.

From these observations, Ghag et al. (8, 10) examined three models for the unit of foaminess using the Buckingham-Pi theorem and assuming that Eq. [1] is valid. They performed the same analysis as that by Zhang and Fruehan (34) but replaced the equilibrium surface tension by (1) the surface tension depression, (2) the Marangoni dilational modulus, and (3) the effective elasticity for solutions following Langmuir behavior. They concluded that the best of the three models was the one using the effective elasticity provided that the solution follows Langmuir behavior. Due to the complexity of the models and the fact that effective elasticity is not available to fully validate the model for a wide range of experimental conditions and solutions, it will not be discussed further.
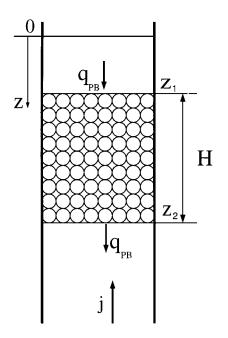
Other authors (22, 37) modeled the steady-state foam thickness based on the mass and momentum conservation equations with applications to slag foaming in steel manufacturing. The validation of those models against experimental data appears to be limited and will not be discussed further.

Finally, a detailed model has been proposed to predict the thickness of pneumatic foams (1). Figure 1 shows a schematic of a typical foam layer formed by injection of gas at the bottom of a vertical column containing a foaming liquid. For this arrangement, Bhakta and Ruckenstein (1) proposed the following

TABLE 1
Summary of Experimental Data for Steady-State Foam Thickness for High-Viscosity Fluids Reported in the Literature

Solution	Dimensions i.d. & H_0	Gas	Nozzle type	Gas flux (mm/s)	σ (mN/m)	μ (mPa·s)	ρ (kg/m³)	T (°C)	r_0 (mm)	Ref.
40%CaO–40%SiO$_2$–5% FeO–15%Al$_2$O$_3$	i.d. = 9.2 cm H_0 = 4.5 cm	Argon	Single & multiple	0 to 50	463.	398	2743	1500	7.8 to 13.5	Zhang and Fruehan (34)
48%CaO–32%SiO$_2$–10% FeO–10%Al$_2$O$_3$	i.d. = 4.1 cm H_0 = 4.2 cm	Argon	Single	0 to 30.	477.2	381	2733	1600	12	Ozturk and Fruehan (29)
75 SiO$_2$–15 NaO$_2$–10 CaO (wt.%) glass	i.d. = 6.5 cm H_0 = 2.0 cm	Air	Single	0 to 2.5	297.7 to 307.7	7450 to 12100	2346.6 to 2358.6	1425 to 1500	15 to 20	Laimbock (21)
Water + 78% to 95% glycerinate + SDBS	i.d. = 10.7 cm H_0 = 16.7 cm	N$_2$	Pyrex disk	0.83 to 1.5	69.5 to 72.3	46.5 to 520.8	1204 to 1251	20	0.7 to 1.1	Ghag et al. (9)
30% FeO–42% SiO$_2$–28% CaO	i.d. = 3.2/5 cm H_0 = N.A.	Argon	Single	0 to 27.0	477.9	1605	3055	1300	12	Ito and Fruehan (15)
3% FeO (CaO/SiO$_2$ = 1.25)	i.d. = 9.2 cm H_0 = 4.5 cm	Argon	Single	0 to 30.3	477.2	381	2733	1500	12	Jiang and Fruehan (18)
0% FeO (CaO/SiO$_2$ = 1.25	i.d. = 9.2 cm H_0 = 4.5 cm	Argon	Single	0 to 40.4	472.8	396	2693	1500	12	Jiang and Fruehan (18)
30%CaO–60%SiO$_2$–10% CaF$_2$	i.d. = 4.1 cm H_0 = 4.5 cm	Argon He, H$_2$	Single	0 to 40.	338	533 [39]	2534	1400 or 1500	13	Zhang and Fruehan (35, 36)
34.78%CaO–33.76%SiO$_2$– 22.52%FeO–8.94%MgO	i.d. = 4.5 cm H_0 = 4 cm	Argon	Single	0 to 67.3	502	270	2958	1600	17	Jung and Fruehan (19)
37.39%CaO–35.57%SiO$_2$ 20.87%FeO–6.17%MgO	i.d. = 4.5 cm H_0 = 4 cm	Argon	Single	0 to 67.4	493	291	2936	1600	17	Jung and Fruehan (19)

FIG. 1. Schematic of a foam layer generated by a bubbling and coordinate system with notations.

expression for z_1 and z_2, the vertical coordinates of the top and bottom of the foam, respectively,

$$\frac{dz_1}{dt} = \frac{\phi(z_1, t)q_{PB}(z_1, t)}{1 - \phi(z_1, t)} \qquad [4]$$

$$\frac{dz_2}{dt} = \frac{j}{\phi(z_2, t)} - q_{PB}(z_2, t), \qquad [5]$$

where j is the superficial gas velocity, $\phi(z, t)$ is the volume fraction of gas (or porosity), and $q_{PB}(z, t)$ is the mass flow rate of liquid through the Plateau border at location z and time t. Since the total foam thickness can be expressed as $H_\infty = (z_2 - z_1)$, one obtains

$$\frac{dH}{dt} = \frac{d(z_2 - z_1)}{dt} = \frac{j}{\phi(z_2, t)} - q_{PB}(z_2, t) - \frac{q_{PB}(z_1, t)\phi(z_1, t)}{1 - \phi(z_1, t)}. \qquad [6]$$

The first term on the right-hand side represents the increase of the foam thickness due to the incoming gas while the last two terms represent the decrease of the foam thickness due to the liquid leaving the foam through the Plateau borders and the gas leaving the foam due to bubble rupture at the top of the foam, respectively.

Assuming that (1) the foam bed consists of dodecahedron bubbles of the same size, (2) the Plateau borders are randomly oriented, (3) the drainage through the Plateau borders due to film thinning is negligible compared to that due to gravity (see Refs. (1, 25) for additional discussion), (4) coalescence of bubbles and Ostwald ripening within the foam are absent, (5) surface tension is constant, (6) the wall effects are negligible, and (7) the foam is

under isothermal conditions, an expression for the volumic flow rate through the Plateau border $q_{PB}(z, t)$ is given by (26, 27)

$$q_{PB}(z, t) = \left(\frac{3}{15}\right) N r n_p a_p u, \qquad [7]$$

where r is the bubble radius, N is the number of bubbles per unit volume, n_p is the number of Plateau borders per bubble, a_p is the cross-sectional area of a Plateau border, and u is the velocity of the fluid through the Plateau border due to gravity drainage. A simplified expression for those parameters has been developed by Narsimhan and co-worker (25, 27) and can be reformulated as follows,

$$N = \frac{3\phi}{4\pi r^3},$$

$$n_p = 10,$$

$$a_p = \frac{4\pi r^3/3}{0.816 r n_p}\left(\frac{1 - \phi}{\phi}\right),$$

$$u = \frac{c_v a_p}{20\sqrt{3}\mu}\left[\rho g + \sigma \frac{d}{dz}\left(\frac{1}{\alpha a_p^{1/2}}\right)\right] \qquad [8]$$

where α is a dimensionless constant[3] (25), and the velocity coefficient c_v (dimensionless) accounts for the mobility of the walls of a Plateau border channel and has been computed by Desai and Kumar (6). In most of their calculations, Ruckenstein and co-worker used $c_v = 1$ (1). Combining Eq. [7] with Eq. [8] yields

$$q_{PB}(z, t) = 3.632 \times 10^{-3} c_v \frac{[1 - \phi(z, t)]^2}{\phi(z, t)}\left\{\frac{\rho g r^2}{\mu}\right.$$

$$\left. + \frac{1.3957}{\alpha}\frac{\sigma r^2}{\mu}\frac{\partial}{\partial z}\left[\left(\frac{\phi(z, t)}{(1 - \phi(z, t))r^2}\right)^{\frac{1}{2}}\right]\right\}. \qquad [9]$$

Equation [9] can be solved numerically and simultaneously with the transient equation for the foam porosity at height z and time t, $\phi(z, t)$ (1). The porosity at the bottom of the foam layer $\phi(z_2, t)$ is assumed to be constant and equal to 0.74. The steady-state foam thickness is then obtained from the limit of the transient calculations ($t \rightarrow \infty$). However, this method for calculating the steady-state foam thickness may be time and resource consuming and thus does not appear to be satisfactory for practical applications. Moreover, the solution has been proven to be highly sensitive to initial conditions (1) that are difficult to obtain either experimentally, analytically, or numerically.

In the present work, an attempt is made to develop a general correlation capable of predicting the steady-state foam thickness for a wide variety of systems having widely different thermophysical properties and average bubble diameters. Instead of using the Buckingham-Pi theorem, the governing equations [6]

---

[3] $\alpha a_p^{1/2}$ represents the radius of curvature of the Plateau border (25).

and [9] for the foam thickness are properly scaled to obtain an expression for the steady-state foam thickness.

Dimensional Analysis

In this study, we assume isothermal conditions and that thermophysical properties are constant across the foam layer. We also assume that limitations and assumptions used to develop Eqs. [6] and [9] are valid. Equations [6] and [9] are nondimensionalized by using the following independent dimensionless variables,

$$z^* = \frac{z}{H_\infty}, \quad r^* = \frac{r}{r_0}, \quad j^* = \frac{j}{(j - j_m)}, \quad t^* = \frac{t}{\tau}, \quad [10]$$

where H_∞ is the steady-state foam thickness, r_0 is the average bubble radius, j_m is the superficial gas velocity of onset of foaming, and τ is the characteristic time for the foam formation. Substituting Eqs. [10] in Eqs. [6] and [9] yields

$$\frac{H_\infty}{\tau}\frac{dH^*}{dt^*}$$

$$= \frac{j - j_m}{\phi(z_2^*)}j^* - 3.632 \times 10^{-3}c_v\frac{\rho g r_0^2}{\mu}r^{*2}$$

$$\times \left[\frac{[1 - \phi(z_2^*, t^*)]^2}{\phi(z_2^*, t^*)} + 1 - \phi(z_1^*, t^*)\right]$$

$$- 5.069 \times 10^{-3}\alpha c_v\frac{\sigma r_0}{\mu H_\infty}r^*\left\{\frac{[1 - \phi(z_2^*, t^*)]^2}{\phi(z_2^*, t^*)}\right.$$

$$\times \frac{\partial}{\partial z^*}\left[\left(\frac{\phi(z^*, t^*)}{(1 - \phi(z^*, t^*))r^{*2}}\right)^{\frac{1}{2}}\right]_{z_2^*} + [1 - \phi(z_1^*, t^*)]$$

$$\left.\times \frac{\partial}{\partial z^*}\left[\left(\frac{\phi(z^*, t^*)}{(1 - \phi(z^*, t^*))r^{*2}}\right)^{\frac{1}{2}}\right]_{z_1^*}\right\}. \quad [11]$$

Further simplification can be obtained by choosing the characteristic time $\tau = H_\infty/(j - j_m)$; then, Eq. [11] becomes

$$\frac{dH^*}{dt^*} = \frac{j^*}{\phi(z_2^*)} - 3.632 \times 10^{-3}c_v\Pi_1 r^{*2}$$

$$\times \left[\frac{[1 - \phi(z_2^*, t^*)]^2}{\phi(z_2^*, t^*)} + 1 - \phi(z_1^*, t^*)\right]$$

$$- 5.069 \times 10^{-3}\frac{\alpha c_v}{\Pi_2}r^*\left\{\frac{[1 - \phi(z_2^*, t^*)]^2}{\phi(z_2^*, t^*)}\right.$$

$$\times \frac{\partial}{\partial z^*}\left[\left(\frac{\phi(z^*, t^*)}{(1 - \phi(z^*, t^*))r^{*2}}\right)^{\frac{1}{2}}\right]_{z_2^*} + [1 - \phi(z_1^*, t^*)]$$

$$\left.\times \frac{\partial}{\partial z^*}\left[\left(\frac{\phi(z^*, t^*)}{(1 - \phi(z^*, t^*))r^{*2}}\right)^{\frac{1}{2}}\right]_{z_1^*}\right\}, \quad [12]$$

where the two dimensionless parameters Π_1 and Π_2 can be identified:

$$\Pi_1 = \frac{\rho g r_0^2}{\mu(j - j_m)} \quad \text{and} \quad \Pi_2 = \frac{\mu H_\infty(j - j_m)}{\sigma r_0}. \quad [13]$$

Π_1 can be interpreted as the ratio of the gravitational force to the viscous force on an average bubble of radius r_0 having a velocity $(j - j_m)$. Π_2 corresponds to the ratio of the viscous force to the surface tension force times the ratio of the steady-state foam characteristic height to the bubble characteristic dimension,

$$\Pi_1 = \frac{\rho g r_0^3}{\mu(j - j_m)r_0} = \frac{\text{gravitational force}}{\text{viscous force}} = \frac{Re}{Fr} \quad [14]$$

$$\Pi_2 = \frac{\mu(j - j_m)r_0}{\sigma r_0} \times \left(\frac{H_\infty}{r_0}\right)$$

$$= \frac{\text{viscous force}}{\text{surface tension force}} \times \left(\frac{H_\infty}{r_0}\right) = Ca\left(\frac{H_\infty}{r_0}\right), \quad [15]$$

where Re, Fr, and Ca are the Reynolds, Froude, and Capillary numbers, respectively, defined as

$$Re = \frac{\rho_c(j - j_m)r_0}{\mu}, \quad Fr = \frac{(j - j_m)^2}{g r_0}, \quad Ca = \frac{\mu(j - j_m)}{\sigma}. \quad [16]$$

The relationship between Π_1 and Π_2 is assumed to follow a power law, i.e.,

$$Ca\left(\frac{H_\infty}{r_0}\right) = K\left(\frac{Re}{Fr}\right)^n, \quad [17]$$

where K and n are constant parameters determined from experimental data. Then, an expression for the steady-state foam thickness H_∞ can be deduced. Note that the choice of a power law to relate the dimensionless numbers Π_1 and Π_2 is arbitrary, but it presents the advantage of capturing a wide variety of possible functional relationships between Π_1 and Π_2.

RESULTS AND DISCUSSION

Results

Experimental data reported in the literature were collected and used to validate the dimensional analysis and to obtain the parameters K and n in Eq. [17]. Table 1 summarizes the experimental conditions used in the studies concerned with the steady-state thickness of foams formed by bubbling gas in a container filled with high-viscosity foaming solutions. Most of the thermophysical properties of iron slags studied by Fruehan and co-workers (15, 16, 18, 19, 34–36) were computed from available models proposed in the literature and summarized in Ref. (24). Data summarized in Table 1 were used to determine the parameters K and n. For the experimental data obtained by

TABLE 2
Summary of Experimental Data for Steady-State Foam Thickness for Low-Viscosity Fluids Reported in the Literature

Solution	Dimensions i.d. and H_0	Gas	Nozzle type	Gas flux (mm/s)	σ (mN/m)	μ (mPa s)	p (kg/m^3)	T (°C)	r_0 (mm)	Ref.
water + 10% glycerinate Marlophen 89 and 812	i.d. = 10 cm H_0 = 45 cm	N_2	Frit glass	0.09 to 0.31	32.0 to 41.1	1.22	1014	20	0.5 to 0.78	Jeelani et al. (17)
water + sucrose AR + glycerol SLR + aerosol OT	i.d. = 6.15 cm H_0 = N.A.	N_2	Multiple	0.09 to 0.82	26	20	1220	30	3.9	Hartland and Barber (12)
water + 10% glycerinate + Marlophen 89 and 812	i.d. = 10 cm H_0 = 45 cm	N_2, NO_x, Xe, CO_2	Frit glass	0.09 to 0.3091	32.0 to 41.1	1.22	1014	20	0.5 to 0.78	Hartland et al. (13)

Zhang and Fruehan (36) for a 30% CaO–60%SiO$_2$–10%CaF$_2$ slag bubbled with argon, hydrogen, and helium, the dimensionless numbers Π_1 and Π_2 were computed assuming that the type of gas has little effect on the surface tension of the binary system gas/slag as observed by Hartland et al. (13) for 10% glycerinate + water +120 mg/L of Marlophen 89 (see Table 2). The steady-state foam thickness from Fruehan and coworkers (15, 16, 18, 19, 34–36) results has been computed to account for the fact that the true foam thickness H_∞ was not measured but instead the distance h from the top of the foam to the initial level of liquid at rest. The foam thickness H_∞ was deduced from the experimental data for h by using the expression (15) $h = H_\infty \phi$ (obtained by writing the mass conservation equation for the liquid phase) and assuming $\phi = 0.8$. Note that the choice of $\phi = 0.8$ is based on experimental data for slag foams (22) and on the observation that the porosity "was between 0.7 and 0.9 and almost independent of the position in the foam" (15). Moreover, parametric studies have shown that values of ϕ between 0.7 and 0.9 have little influence on the results both qualitatively and quantitatively. Indeed, the values obtained for the parameter K are 2932, 2905, and 2881, and −1.79, −1.80, and −1.81 for the parameter n, using the values of porosities $\phi = 0.7, 0.8$,
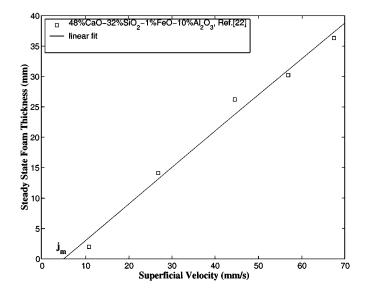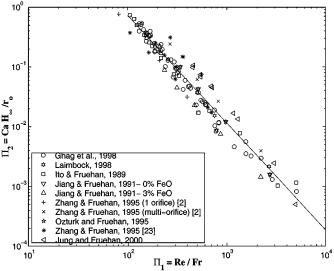
and 0.9, respectively. Thus, considering the experimental uncertainties and that of the thermophysical properties, the choice of $\phi = 0.8$ to treat Fruehan and co-workers' data seems to be acceptable.

The superficial gas velocity for the onset of foaming j_m was determined assuming a linear relationship between the steady-state foam thickness H_∞ and the gas flux j such that $H_\infty = a(j - j_m)$ as shown in Fig. 2.

From Table 1 one can see that experimental studies have covered a wide range of density, viscosity, surface tension, and average bubble radius for more than 120 experimental data points. The dimensionless parameters $\Pi_1[=Re/Fr]$ and $\Pi_2[= Ca(H_\infty/r_0)]$ cover the range of 80 to 5030 and of 5×10^{-4} to 0.76, respectively. Figure 3 shows the relationship between the dimensionless parameters Π_1 and Π_2. Equation [17] appears to fit experimental data over a wide range of thermophysical properties with $K = 2905$ and $n = -1.80$ with a correlation coefficient $R^2_{corr} = 0.95$. In other words, the following relationship between the two dimensionless numbers has been determined:

$$\frac{H_\infty}{r_0} = \frac{2905}{Ca}\left(\frac{Fr}{Re}\right)^{1.80}. \qquad [18]$$

FIG. 2. Steady-state foam thickness vs superficial argon velocity (19).

FIG. 3. Correlation of dimensionless numbers Π_2 vs Π_1.

Equation [18] is general and should be preferred but to compare the present model with experimental findings, it is expressed in dimensional form:

$$H_\infty = 2905 \frac{\sigma}{r_0^{2.60}} \frac{[\mu(j - j_m)]^{0.80}}{(\rho g)^{1.80}}. \qquad [19]$$

The following is evident from Eq. [19]:

• The steady-state foam thickness H_∞ appears to be proportional to $(j - j_m)^{0.80}$, confirming the assumption made in determining the minimum superficial gas velocity for foaming j_m, i.e., $H_\infty \propto (j - j_m)$. The velocity j_m should be determined iteratively in general, but this was not judged necessary due to the proximity of the exponent 0.80 to unity and due to the experimental uncertainty in both the thermophysical properties and the experimental conditions; therefore, j_m in Eqs. [18] and [19] is obtained by assuming a linear relationship between H_∞ and $(j - j_m)$.
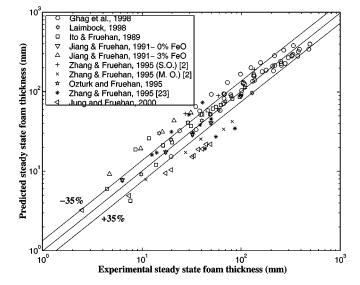• The steady-state foam thickness increases with an increase in the superficial gas velocity j.
• As the viscosity of the liquid phase μ increases, the drainage rate is reduced, the lamellae become thicker and more stable, and thus the foam thickness increases.
• In contrast, the gravity and/or an increase in the liquid density ρ causes the foam to drain faster and to reduce its steady-state thickness.
• The effect of surface tension appears to be in contradiction to experimental observations: it has been observed that an increase in the surface tension σ tends to reduce the steady-state foam thickness (11, 15). This can be interpreted based on the fact that a decrease in the surface tension reduces the interfacial energy and, therefore, increases the foam stability and the steady-state foam thickness. The contradiction is evident if we assume that the surface tension and the average bubble radius are independent, but in reality they are not. Indeed, when considering the effect of the surface tension on the foam thickness as suggested by Eq. [19], one should account for the effect of the bubble radius as well and, therefore, the ratio $\sigma/r_0^{2.60}$ represents the effect of surface tension. If one assumes that the pressure in the bubble is constant and equal to the pressure of injection in the bubbles, the Young–Laplace equation indicates that the bubble radius is proportional to the surface tension. This has been confirmed by Ogawa et al. (28) who observed experimentally that the bubble radius increases linearly with the surface tension. Thus, Eq. [19] suggests that if the surface tension decreases, the bubble radius decreases by the same order, and the ratio $\sigma/r_0^{2.60}$ increases. Hence, according to Eq. [18], the foam thickness increases, as the surface tension decreases in agreement with experimental observations.

Figure 4 compares the steady-state foam thickness obtained experimentally and calculated from Eq. [19]. One can see that most of the experimental data for highly viscous fluids are predicted by the present model within ±35% error. Note that, for molten slags, experimental uncertainties are about ±2% for den-

FIG. 4. Comparison between experimental data and predictions of the steady-state foam thickness. S.O. stands for single-orifice and M.O. for multiple orifice nozzle.

sity, ±10% for surface tension, and about ±25% for viscosity (24); therefore, models predicting those properties should not be expected to be more accurate. The biggest discrepancies encountered between the experimental steady-state foam thickness and the predictions of the model correspond to studies for which thermophysical properties were not measured but estimated from simple relations (15, 16, 18, 19, 34–36) and for which the bubble radius was visually determined (18, 19). On the other hand, studies for which thermophysical properties of the solutions were measured (9, 21) show better agreement. Note also that the discrepancies appear to be higher for small steady-state foam thicknesses, i.e., for superficial gas velocities close to j_m. Consequently, given the uncertainty of the thermophysical properties and of the experimental measurements (in particular, that for the average bubble radius) and given the wide range of thermophysical properties and experimental conditions, the agreement appears to be remarkably good.

Discussion

Several parameters have been identified in the literature as having an influence on the steady-state foam thickness: (i) the thermophysical properties of the solutions (density, viscosity, and surface tension), (ii) the bubble radius (9, 34), (iii) the temperature (5, 29) or the temperature gradient across the foam layer, (iv) the dimensions of the container (18), (v) the initial liquid height or volume at rest (22, 29, 37), (vi) the type of gas injected (13, 36), (vii) the pressure and composition of the surrounding atmosphere (21), and (viii) the solid particles that may be present in the solution (35). The effects of several of these parameters are discussed in the next few subsections. The present study is concerned with two-phase systems, and the effect of a third phase, like solid particles, will not be considered.
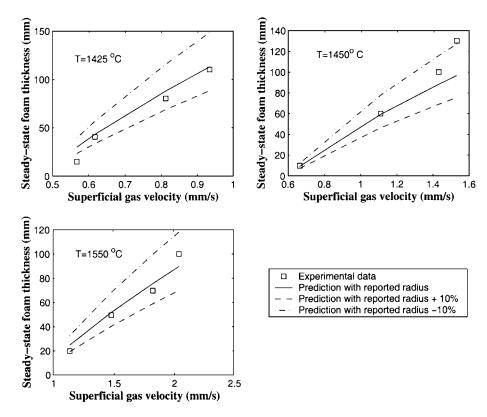
FIG. 5. Influence of the bubble radius on the model predictions for glass foams (21).

Effect of the Bubble Radius

A detailed study on foaming (9) reports the size distributions of bubbles reaching the foam/liquid interface using more than 200 samples. For a solution of water–85 wt% glycerol and surfactants causing a surface tension depression[4] of 5 mN/m, the mean radius of 0.835 mm and a standard deviation of 0.105 mm were recorded; i.e., in terms of 95% confidence intervals, the bubble radius is 0.835 mm ± 24%. Thus, the bubble size distribution has rather wide tails around the mean value, and this should be accounted for to accurately predict the steady-state foam thickness. However, in this work, only the average bubble radius was considered and assumed to be independent of the superficial gas velocity, bearing in mind that it is a first-order approach and based on the conclusion of Narsimhan and Ruckenstein (26) that "the symplifying assumption of equal size bubbles can be employed for the prediction of the stability of the foam bed when the inlet bubble size distribution is narrow, especially at high superficial gas velocity, high viscosities, larger inlet mean bubbles sizes."

Experimentally, different average bubble radii can be obtained via different injection systems, e.g., multiorifice nozzles produce smaller bubbles than single-orifice nozzles (34), and gas

injected through porous materials produces even smaller bubbles (see Table 1). It is evident from Eq. [19] that the average bubble radius has a significant influence on the foam thickness due to an associated exponent of 2.60. Figure 5 compares the experimental steady-state foam thickness obtained for glass foams (21) with the model predictions using three different radii: the reported radius and the reported radius with ±10% deviation. One can see that the predictions vary significantly depending on the average bubble radius used and that, in this particular case, the experimental data lie within the prediction range. These observations provide further confidence in the model but also call for a more refined model that explicitly accounts for the bubble size distribution rather than using the average bubble radius.

Effect of Temperature

Cooper and Kitchener (5) found that foam stability increases with decreasing temperature. They attributed this effect to a higher viscosity as the temperature decreases. Actually, the temperature has an effect on all the thermophysical properties of the solution, but its effect on viscosity is by far more significant than that on the density and the surface tension. Our study uses experimental data taken over a wide range of temperatures for different fluids with thermophysical properties that behave distinctly in response to changes in the temperature (see Table 1), and predictions appear to be satisfactory. Therefore, the model developed in this study captures, in a satisfactory

---

[4] The surface tension depression $\Delta\sigma$ is defined as the difference between the surface tension of the solution without surfactant σ_0 and that with surfactants σ, i.e., $\Delta\sigma = \sigma_0 - \sigma$.

manner, the effect of the temperature on the steady-state foam thickness. In glass melting and other industrial furnaces, the foam layer may be subject to a large temperature gradient but its effect on the steady-state foam thickness remains to be explored.

Effect of the Container Dimensions and the Initial Liquid Height

As already mentioned, experimental data indicate that the container inside diameter has no influence on the steady-state foam thickness of iron slags if it is larger the 3 cm with a mean radius of 12 mm (15). In more general terms, one can state that the effects of the container diameter become negligible when the ratio of the container diameter to bubble diameter is sufficiently large. However, experimental data do not permit the definition of general criteria for the limit of influence of the container size on the steady-state foam thickness. The experimental data used in the present work corresponds to such conditions (see Table 1 and it is assumed that the wall effect is negligible (i.d. >3 cm). Ozturk and Fruehan (29) found that the foaming index increases slightly with the initial slag depth and concluded that the steady-state foam thickness "is almost independent of the slag volume," but recognized that more experiments are needed to fully assess the effect of the initial liquid height. However, additional systematic studies showed that the steady-state foam thickness increases with the increase in the initial liquid height (22, 37). On the other hand, Lin and Guthrie (22) observed that the initial liquid height had no effect for large initial liquid depth (≥30 cm for water/air systems).

The correlation developed in the present work does not use explicitly the initial liquid height; however, we speculate that this height has an influence on the steady-state foam thickness through the superficial gas velocity for the onset of foaming j_m. Indeed, if the liquid depth is large enough, bubbles have time to reach their terminal velocity and the onset of foaming should not depend significantly on the initial liquid height. In contrast, if the initial liquid depth is small, the velocity at which bubbles reach the interface will depend on the initial liquid depth. Note that, in the present study, j_m has been determined experimentally; i.e., if our speculation is correct, the effect of the initial liquid height, if any, has been accounted for. Although experimental work showed the existence of non-zero superficial gas velocity for the onset of foaming j_m (9, 21), to the best of our knowledge, no model for j_m has been proposed in the literature.

Effect of the Surrounding Atmosphere

The present study used data for foams generated under air at atmospheric pressure. However, two parameters characterizing the surrounding atmosphere can influence the steady-state foam thickness: (i) the total pressure and (ii) the atmosphere chemical composition. An increase in the total pressure imposed at the top of the foam layer limits significantly the steady-state foam thickness (20). Cable et al. (4) studied the foaming behavior of binary silicate melts and conclude that the atmosphere compo-

sition had a significant effect on the foam. They experimentally observed that no glass foam was observed in a pure nitrogen atmosphere and that glass foams are more stable in a pure oxygen atmosphere, confirming visual observations (21). Kappel et al. (20) also showed that increasing the partial pressure of water on top of the glass foam destabilizes it. Injection of different gases on the top of the foam is a technique widely used in glass manufacturing to destroy the foam layer formed on the surface of the glass melt. The effect of the surrounding atmosphere has not been fully evaluated experimentally and should be further assessed.

Effect of the Gas Type Contained in the Bubbles

The thermophysical properties of the system affected by the type of gas bubbled in the solution are the surface tension, the gas diffusion coefficient, and the gas solubility in the liquid phase. For viscous liquids, foam lamellae are thick due to slow drainage; therefore, Ostwald ripening and coalescence should not have a significant effect on the steady-state foam thickness. This is confirmed by the present work: data for relatively high viscosity fluids ($\mu > 46$ mPas) reported in Fig. 3 and summarized in Table 1 follow the same trend and are characterized by the same experimental parameters K and n, even though obtained for different gases (air, helium, hydrogen, argon, and nitrogen). The effect of the type of gas on viscous fluids has been studied by Zhang and Fruehan (36) who showed that the steady-state thickness of slag foam was affected neither by the gas pressure nor by the density of the gas inside the bubbles. Instead, the unit of foaminess obtained for different gases varied linearly with the viscosity of the gas contained in the bubbles, but the authors did not propose any physical interpretation of this effect. They also observed that there was "no change in the appearance as well as the size of the bubble cells in the foam no matter what type of gas was used." Further, they reported a relatively narrow bubble size distribution centered around a mean value of 13 mm ± 11.5%. These experimental observations indicate that no coalescence or Ostwald ripening was taking place within the slag foam (viscous fluid). Considering the uncertainties for the thermophysical properties and for the experimental data, one can conclude that the type of gas contained in the bubbles has little effect on the behavior of foams generated from viscous liquids. Then, the model developed in the present work gives satisfactory results.
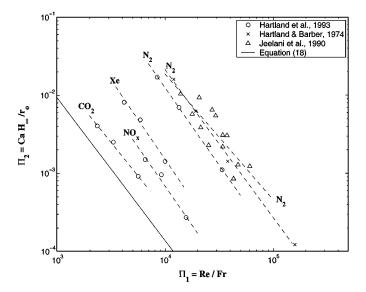
For low-viscosity fluids, however, such as those used by Hartland and co-workers (12, 13, 17), the foam lamellae become thin and coalescence and gas diffusion effects may play a significant role. Table 2 summarizes the conditions of studies concerned with the steady-state thickness of low-viscosity fluids. Hartland et al. (13) showed that, for low-viscosity solutions, the foam height was reduced for gases of high solubility due to interbubble gas diffusion that tend to create bigger and less stable bubbles which can coalesce or burst within the foam and cause the foam to collapse. Results reported by Hartland and co-workers (12, 13, 17) for different gases injected in different low-viscosity

TABLE 3
Values of Parameters K and n Obtained from Experimental Data and Relevant Properties for Different Gases Injected in Low-Viscosity Fluids

Solution	Concentration	Gas	σ (mN/m)	μ (mPa s)	ρ (kg/m^3)	r_0 (mm)	K	n	Ref.
water + 10% glycerinate + Marlophen 89	120	N_2	32.1	1.22	1014	0.5	2.94×10^6	-2.04	Jeelani et al. (17)
water + 10% glycerinate + Marlophen 89	80	N_2	35.4	1.22	1014	0.5	4.13×10^8	-2.45	
water + 10% glycerinate + Marlophen 89	40	N_2	41.1	1.22	1014	0.5	4.94×10^5	-1.88	
water + 10% glycerinate + Marlophen 812	80	N_2	35.4	1.22	1014	0.5	1.06×10^7	-2.08	
water + sucrose AR + glycerol SLR + aerosol OT	120	N_2	26	20	1220	3.9	8.37×10^5	-1.90	Hartland and Barber (12)
water + 10% glycerinate + Marlophen 89	120	N_2	32.1	1.22	1014	0.5	1.05×10^6	-1.98	Hartland et al. (13)
water + 10% glycerinate + Marlophen 89	120	NO_x	31	1.22	1014	0.5	6.85×10^4	-2.00	
water + 10% glycerinate + Marlophen 89	120	Xe	31.52	1.22	1014	0.4	02.19×10^5	-2.04	
water + 10% glycerinate + Marlophen 89	120	CO_2	31.13	1.22	1014	0.3	2.82×10^3	-1.73	

solutions are reproduced in Fig. 6 in terms of the dimensionless numbers Π_1 and Π_2. Relevant experimental conditions and the experimental constants K and n are summarized in Table 3. Note that for data reported by Hartland et al. (13) the size distribution and the average bubble radius change drastically along the foam height. More precisely, the bubble size distribution has a narrow bell shape at the bottom of the foam and flattens out toward the top as small bubbles become smaller and large bubbles become larger due to interbubble gas diffusion and bubble coalescence. Therefore, the discrepancies between the experimental data for low-viscosity fluids and the present work (Eq. [17]) can be explained by the fact that the bubble size distribution within the foam is described by a single parameter, r_0, taken as the average bubble radius at the bottom of the foam layer. While this approach seems to be sufficient for highly viscous fluids for which the porosity and the bubble size distribution are almost uniform across the foam layer (15, 36), it is not satisfactory for low-

viscosity fluids where bubble coalescence and Ostwald ripening are significant.

Moreover, it is worth noting that for the low-viscosity solutions summarized in Tables 2 and 3, the parameter K changes with the type of gas while n is almost the same for all gases and is close to the exponent 1.80 found for highly viscous fluids. It is also interesting to remark that experimental data obtained for nitrogen bubbled in different low-viscosity fluids and with bubbles of different radii occupy the same region of the Π_2 vs Π_1 plot (Fig. 6).

Finally, these findings tend to indicate that the deviation from the model developed in the present work should depend on the bubble size distribution and on the intrinsic properties of the gas phase. In other words, a third dimensionless number should be introduced by extending Eq. [6] for the transient foam thickness to account for Ostwald ripening, bubble coalescence, and other phenomena involving the gas phase and for a nonuniform bubble size distribution within the foams. Note that these considerations have been neglected in the development of Eqs. [6] and [9] proposed by Bhakta and Ruckenstein (1) and by Narsimhan and Ruckenstein (25, 27). The third dimensionless number would, then, depend on the thermophysical properties of the gas (e.g., solubility in the liquid phase, diffusion coefficient, etc.) and hopefully enable one to collapse the data on a single line as presented in this paper for high-viscosity fluids.

CONCLUSIONS

This paper presents an approach to predict the thickness of pneumatic foams under steady-state and isothermal conditions. A dimensional analysis has been performed based on the governing equation for the transient foam thickness. Two dimensional numbers have been identified as necessary to describe the formation and stability of this type of foam:

FIG. 6. Correlation of dimensionless numbers Π_1 and Π_2 for different gases injected into low-viscosity solutions.

$$\Pi_1 = \frac{Re}{Fr} \quad \text{and} \quad \Pi_2 = Ca \times \frac{H_\infty}{r_0}.$$

Physical interpretation of the dimensionless numbers has been proposed and the power law type relation has been assumed between Π_1 and Π_2. Experimental data have been used to find the empirical parameters of the correlation (i.e., $\Pi_2 = K \Pi_1^n$). The resulting semi-empirical model has been validated by comparing its predictions with available data covering a wide range of viscosity, density, surface tension, gas superficial velocity, and average bubble radius with the following conclusions:

1. The relationship between the dimensionless parameters can be expressed as

$$\frac{H_\infty}{r_0} = \frac{2905}{Ca} \left(\frac{Fr}{Re} \right)^{1.80}.$$

This equation is valid for foams formed from high-viscosity liquids bubbled with nitrogen, air, and argon injected through single-orifice or multiorifice nozzles or a porous medium and featuring the following thermophysical property and experimental condition ranges:

- $46 < \mu < 12100$ mPas,
- $1200 < \rho < 3000$ kg/m^3,
- $69.5 < \sigma < 478$ mN/m,
- $0 < j < 40$ mm/s,
- $0.7 < r_0 < 20$ mm.

2. Comparison between the developed semi-empirical correlation and the experimental data yields reasonable agreements (within 35% error) given the broadness of the bubble radius distribution around the mean value and the uncertainty of the experimental data and of the thermophysical properties.

3. Predictions are very sensitive to the average bubble radius and a more refined model is still needed which should be supported by careful experimental studies.

4. The effects of the initial liquid height and of the surrounding atmosphere and that of the type of gases contained in the bubbles remain to be explored.

APPENDIX: NOMENCLATURE

a_p	Cross-sectional area of a Plateau border
b_h	Parameter in Eq. [2]
c_v	Dimensionless parameter, Eq. [8]
D_0	Average bubble diameter in the foam ($=2r_0$)
g	Specific gravity
H	Foam thickness
H_0	Initial height of the liquid in the container
H_∞	Steady-state foam thickness
j	Superficial gas velocity
j_{cr}	Critical superficial gas velocity
j_m	Superficial gas velocity for onset of foaming
K	Constant defined experimentally, Eq. [17]
n	Constant defined experimentally, Eq. [17]
n_p	Number of Plateau borders per bubble

N	Number of bubbles per unit volume
q_{PB}	Mass flow rate through the Plateau border
r_0	Average bubble radius in the foam
R	Universal gas constant $= 8.314$ J/(mol K)
R_{corr}^2	Correlation coefficient
T	Temperature
t	Time
u	Velocity of the fluid through the Plateau border due to gravity drainage
z	Downward vertical elevation (see Fig. 1)

Dimensionless Numbers

Ca	Capillary number, defined in Eq. [16]
Fr	Froude number, defined in Eq. [16]
Re	Reynolds number, defined in Eq. [16]

Greek Symbols

α	Dimensionless parameter, Eq. [8]
β	Constant
ϕ	Foam porosity (volumetric gas fraction)
μ	Dynamic viscosity of the liquid phase
Ω	Unit of foaminess, constant defined experimentally, Eq. [1]
$\Pi_{1,2}$	Dimensionless groups
ρ	Density
σ	Surface tension
τ	Characteristic time to reach steady-state conditions

Subscripts

1	Refers to the top of the foam layer
2	Refers to the bottom of the foam layer

Superscript

$*$	Refers to dimensionless properties

REFERENCES

1. Bhakta, A., and Ruckenstein, E., *Adv. Colloid Interface Sci.* **70,** 1–124 (1997).
2. Bikerman, J. J., *Trans. Faraday Soc.* **38,** 634–638 (1938).
3. Boulton-Stone, J. M., and Blake, J. R., *J. Fluid Mech.* **254,** 437–466 (1993).
4. Cable, M., Rasul, C. G., and Savage, J., *Glass Technol.* **9**(2), 25–31 (1968).
5. Cooper, C. F., and Kitchener, J. A., *J. Iron Steel Inst.* Sept., 48–55 (1959).
6. Desai, D., and Kumar, R., *Chem. Eng. Sci.* **37**(9), 1361–1370 (1982).
7. Fedorov, A. G., and Viskanta, R., *Phys. Chem. Glasses* **41**(3), 127–135 (2000).
8. Ghag, S. S., Hayes, P. C., and Lee, H.-G., *ISIJ Int.* **38,** 1208–1215 (1998).

9. Ghag, S. S., Hayes, P. C., and Lee, H.-G., *ISIJ Int.* **38,** 1201–1207 (1998).

10. Ghag, S. S., Hayes, P. C., and Lee, H.-G., *ISIJ Int.* **38,** 1216–1224 (1998).

11. Hara, S., Takayuki, T., and Ogino, K., *J. Iron Steel Inst. Jpn.* **12,** 2182–2187 (1989).

12. Hartland, S., and Barber, A. D., *Trans. Inst. Chem. Eng.* **52,** 43–52 (1974).

13. Hartland, S., Bourne, J. R., and Ramaswami, S., *Chem. Eng. Sci.* **48,** 1723–1733 (1993).

14. Hrma, P., *J. Colloid Interface Sci.* **134**(1), 161–168 (1990).

15. Ito, K., and Fruehan, R. J., *Metall. Mater. Trans. B* **20,** 509–514 (1989).

16. Ito, K., and Fruehan, R. J., *Metall. Mater. Trans. B* **20,** 515–521 (1989).

17. Jeelani, S. A. K., Ramaswami, S., and Hartland, S., *Trans. Inst. Chem. Eng. A* **68,** 271–277 (1990).

18. Jiang, R., and Fruehan, R. J., *Metall. Mater. Trans. B* **22,** 481–489 (1991).

19. Jung, S.-M., and Fruehan, R. J., *ISIJ Int.* **40,** 348–354 (2000).

20. Kappel, J., Conradt, R., and Scholze, H., *Glastech. Ber.* **60**(6), 189–201 (1987).

21. Laimbock, P. R., "Foaming of glass melts." Ph.D. thesis, Technical University of Eindhoven, Eindhoven, The Netherlands, 1998.

22. Lin, Z., and Guthric, R. I. L., *Iron Steelmaker* **22**(5), 67–73 (1995).

23. McElroy, R., "Air release from mineral oils." Ph.D. thesis, Department of Pure and Applied Chemistry, Strathclyde University, 1978.

24. Mills, K. C., and Keene, B. J., *Int. Mater. Rev.* **32**(1–2), 1–120 (1987).

25. Narsimhan, G., *J. Food Eng.* **14,** 139–165 (1991).

26. Narsimhan, G., and Ruckenstein, E., *Langmuir* **2,** 494–508 (1986).

27. Narsimhan, G., and Ruckenstein, E., *Langmuir* **2,** 230–238 (1986).

28. Ogawa, Y., Huin, D., Gaye, H., and Tokumitsu, N., *ISIJ Int.* **33**(1), 224–232 (1993).

29. Ozturk, B., and Fruehan, R. J., *Metall. Mater. Trans. B* **26,** 1086–1088 (1995).

30. Pattle, R. E., *J. Soc. Chem. Ind.* **69,** 368–371 (1950).

31. Roth, R. E., Jiang, R., and Fruehan, R. J., *Trans. Iron Steel Soc. AIME* **14,** 95–103 (1993).

32. Watkins, R. C., *J. Inst. Pet.* 106–113 (1973).

33. Wu, K., Chu, S., Qian, W., and Niu, Q., *Steel Res.* **70**(7), 248–251 (1999).

34. Zhang, Y., and Fruehan, R. J., *Metall. Mater. Trans. B* **26,** 803–812 (1995).

35. Zhang, Y., and Fruehan, R. J., *Metall. Mater. Trans. B* **26,** 813–819 (1995).

36. Zhang, Y., and Fruehan, R. J., *Metall. Mater. Trans. B* **26,** 1089–1091 (1995).

37. Zhu, M.-Y., and Sichen, D., *Steel Res.* **71**(3), 76–82 (2000).